https://doi.org/10.5194/egusphere-2022-501
Preprint. Discussion started: 27 June 2022


# Impact of the sampling procedure on the specific surface area of snow measurements with the IceCube

Julia Martin[1,2] and Martin Schneebeli[2]

[1]Alfred Wegener Institute, Helmholtz Centre for Polar and Marine Research (AWI), Telegrafenberg, 14473 Potsdam, Germany
[2]WSL Institute for Snow and Avalanche Research SLF, Flüelastrasse 11, 7260 Davos Dorf, Switzerland

**Correspondence:** Julia Martin (julia.martin@awi.de)

**Abstract.** The specific surface area (SSA) of snow is directly measured by X-ray computed tomography or indirectly using the reflectance of near-infrared light. The IceCube is a well-established spectroscopic instrument using a near-infrared wavelength of $1310\,\mathrm{nm}$. We compared the SSA of six snow types measured with both instruments. The IceCube measured significantly higher values with a relative percentage difference between 20 to $52\,\%$ for snow types with an SSA between 5 to $25\,\mathrm{m^2\,kg^{-1}}$. There is no significant difference for snow with an SSA between 30 to $80\,\mathrm{m^2\,kg^{-1}}$. The difference is statistically significant between snow types but not uniquely related to the SSA. We suspected that artificially created particles were the source of the difference. These were sampled, measured and counted. Numerical simulations with radiation transfer solver TARTES confirm the observation.

## 1 Introduction

The specific surface area of snow (SSA) is the most relevant parameter beyond the snow density for the structural characterisation of snow (Morin et al., 2013). The SSA is the surface of snow grains per mass in units of $\mathrm{m^2\,kg^{-1}}$ or over ice density in $\mathrm{m^{-1}}$. The SSA changes due to metamorphism and is about $100\,\mathrm{m^2\,kg^{-1}}$ for new snow and less than $2\,\mathrm{m^2\,kg^{-1}}$ for melt-freeze layers. SSA is relevant for snow chemistry, radiation transfer in snow, and mechanical properties ((Domine et al., 2008). For determining SSA indirectly, the IceCube (IC) is an efficient, transportable, optical device operating at $1310\,\mathrm{nm}$ wavelength, which derives the SSA from the reflectance of snow. It uses a specific wavelength to invert from the reflectance of snow to the optical grain size of the snow (Domine et al., 2007; Gallet et al., 2014). Computed microtomography (micro-CT) is a high-resolution imaging technique to measure SSA from geometry (Kerbrat et al., 2007). Coincidental measurements of the SSA of snow with both the IC and the micro-CT showed inconsistent results. This study aims to elucidate the reasons for the observed differences. We focus here on small particles on the prepared snow surface used for the reflectance measurements. We furthermore investigate the amount and size distribution of these particles and use a numerical simulation to support our

https://doi.org/10.5194/egusphere-2022-501
Preprint. Discussion started: 27 June 2022


hypothesis. Black carbon is only very slightly absorbing in the near-infrared, so it can be excluded as a source of the difference on the reflectance of the IC.

## 2 Methodology

### 2.1 Snow sampling and SSA measurements

We use five different snow types for this study (5 - 25 $\mathrm{m^2\,kg^{-1}}$). Additionally we take into account a data set with an artificial snow type (30 - 80 $\mathrm{m^2\,kg^{-1}}$) to cover a broad range of SSA. Type A is a homogeneous alpine settled snow with a decomposed, rounded grain shape, sized 0.5 to 1.5 mm. Type B is snow of type A stored for 13 days at $-15\,^{\circ}\mathrm{C}$ in the cold lab under compacting weights. The grain shape is small rounded, the grain size is medium with 0.5 to 1 mm and the structure behaves more brittle than type A. Type C has large rounded, faceted shaped grains with a size between 1 and 2.5 mm. Type D is snow with large rounded grains and a size of 1 to 2 mm. Type E is refrozen wet snow and has grains larger than 2.5 mm. Type E is rather heterogeneous. For SSA sampling with the IC and micro-CT a homogeneous layer of approximately 6 cm was necessary. The homogeneity of the sample was checked using SnowMicroPen measurements (Schneebeli and Johnson, 1998). We cut off the unsuitable material above the sampling layer and brushed the surface gently to eliminate loose particles. Our sampling starts by taking an IC sample following the default method by Gallet et al. (2009) and described in the IC manual (A2 Photonic Sensors (2014)). The SSA is measured, and afterwards, the sample is gently tilted over a petri dish to remove potentially remaining loose particles within the surface area. That particle amount is weighted (micro scales $\pm 0.01$ g) and photographed (Leica Z16 APO). The mass of the loose particles is divided by the surface area of the sample holder to receive the specific mass ($M_{spec}$). Next up, a second SSA is now measured with this IC sample without any loose particles. For comparison, we take a micro-CT sample out of each IC sample. For reference, we additionally perform micro-CT samples next to the IC samples within the undisturbed snow structure. The IC has a sampling kit with a 60 mm diameter holder. We manufactured a similar kit for the micro-CT that consists of a 30 mm diameter sample holder to improve the resolution. This micro-CT kit reproduces the mechanical treatment of the IC sampling process to scan in-situ broken particles on the surface produced during the specific sampling procedure, together with the snow structure deeper in the sample middle. All micro-CT measurements were performed using the computer tomography system working in a cold laboratory at $-15\,^{\circ}\mathrm{C}$ (Scanco Medical $\mu$CT40 or $\mu$CT80). For comparison with the IC, samples were measured with $\mu$CT40 (55 kVp energy, 15 µm nominal resolution, 145 µA intensity: type A; 55 kVp, 18 µm $\mu$m, 145 µA: B-E). The micro-CT sampling kit data set was measured with $\mu$CT80 (55 kVp, 15 µm, 145 µA: A-E). The SSA was computed using the standard segmentation technique as described in (Hagenmuller et al., 2016).

### 2.2 Grain survey

We examined and photographed the loose particles created by sample preparation in a Petri dish to study their influence on the surface of the IC sample. The Petri dish was subdivided into eight sections and eight circles. Random numbers were generated

https://doi.org/10.5194/egusphere-2022-501
Preprint. Discussion started: 27 June 2022


to receive eight coordinates per sample, resulting in 40 pictures per snow type sample. This procedure guaranteed unbiased pictures without a particular preference for the shape. Eight pictures with about 100 grains in total for snow of types B, D, and E were randomly chosen to obtain the grain size distribution. For snow types A and C, 12 pictures were chosen to obtain the same number of grains. The length and width of every particle were measured with ImageJ (Abràmoff et al., 2004), and the optical diameter $d_{opt}$ and SSA ($SSA_{mass}$) were calculated, assuming the main grain shape to be ellipsoidal. The total amount of measured grains, the median diameter, the median SSA, the optical diameter $d_{opt}$ and the $M_{spec}$ for each snow type were recorded in Table 3.

### 2.3 TARTES simulations

To simulate the influence of a layer of artificial particles on top of a substrate snow layer we use the TARTES model (Two-streAM Radiative TransfEr in Snow) (Libois et al., 2013). The SSA of the particle layer on top is the median SSA calculated from the grain examination for each snow type. The density of the particle layers ($\rho_{layer}$) was set to $200\,\mathrm{kg\,m^{-3}}$. We used the average SSA ($SSA_{substrate}$, Tab. 3) and average density ($\rho_{substrate}$, Tab. 3) of the micro-CT samples out of the IC samples (CT out of IC) as input for the substrate layer below and the synthetic substrate depth was set to $1\,\mathrm{m}$. The simulations used $1310\,\mathrm{nm}$ wavelength to study the particle influence of the IC operating wavelength and $950\,\mathrm{nm}$ wavelength as an approximation to the NIR photography. The first step was to calculate the diffuse albedo for the two layer simulation using the albedo function of the TARTES python module. As the desired output variable was the SSA a conversion needed to be applied to the diffuse albedo data set. Hence, a synthetic SSA data set for both wavelengths was produced. They were used for a poly fitting procedure. A five degree polynomial was deemed to be adequate to describe the relationship between the calculated diffuse albedo and SSA.

## 3 Results

Figure 1a shows that the SSA of the nature-identical new snow was the same for both methods, IC and CT. We measured a lower SSA with the micro-CT for all sintered snow types, independent of the SSA, compared to IC (Fig. 1b, details in Table 3 and Fig.2). We also measured a lower SSA in the micro-CT if we measured the prepared flat surface compared to the undisturbed middle of the sample (Fig. 1c). We present now the detailed results for the different treatments of the samples. The nature-identical new snow has no significant difference between the methods (n = 45, p-value: .43, p<0.05). The sintered snow types A, B, C, D show a significant difference at the 0.05-level between IC and micro-CT ($\overline{SSA}$ (IC + particles) vs. $\overline{SSA}$ (CT out of IC), see Tab.3 and Fig.2). Snow type E (four micro-CT samples) had a larger scatter both in IC and micro-CT and is therefore not statistically different. However, the SSA is 24% smaller measured by the micro-CT compared to the IC. The treatment "removing loose particles" (IC - particles) leads to a slight decrease in the IC measurements. The difference between these two sampling steps (IC + particles vs. IC - particles, Tab. 3) is not significant for types A, B and E and is significant for types C and D. Comparing these (IC - particles) with the micro-CT samples (CT out of IC) the difference is not significant for types A, B, C and D. The difference between the micro-CT samples (CT out of IC) and the micro-CT samples taken out of the same snow block next to the IC samples (CT reference) is not significant for types A, B, and E. There is only one reference

https://doi.org/10.5194/egusphere-2022-501
Preprint. Discussion started: 27 June 2022


sample for type C.

Most surface samples measured with the micro-CT sampling kit (Fig. 1c and Fig. 3) show a higher SSA than those in the undisturbed middle of each sample. The difference is significant for types C and D. For types A and B, the SSA measured at the sample's surface is higher than those measured in the middle, but not significantly. For the heterogeneous refrozen wet snow of type E, the SSA at the surface is lower than in the middle. Type D shows the highest mean SSA difference with 28%. Fig. 3 shows the three-dimensional reconstruction of this particular snow sample. Fig 3a is the sample surface, and 3b displays the middle. The fragmented artificial particles (less than $0.5\,\mathrm{mm}$) point out compared to the undisturbed snow structure with a size of $1\,\mathrm{mm}$ and more.

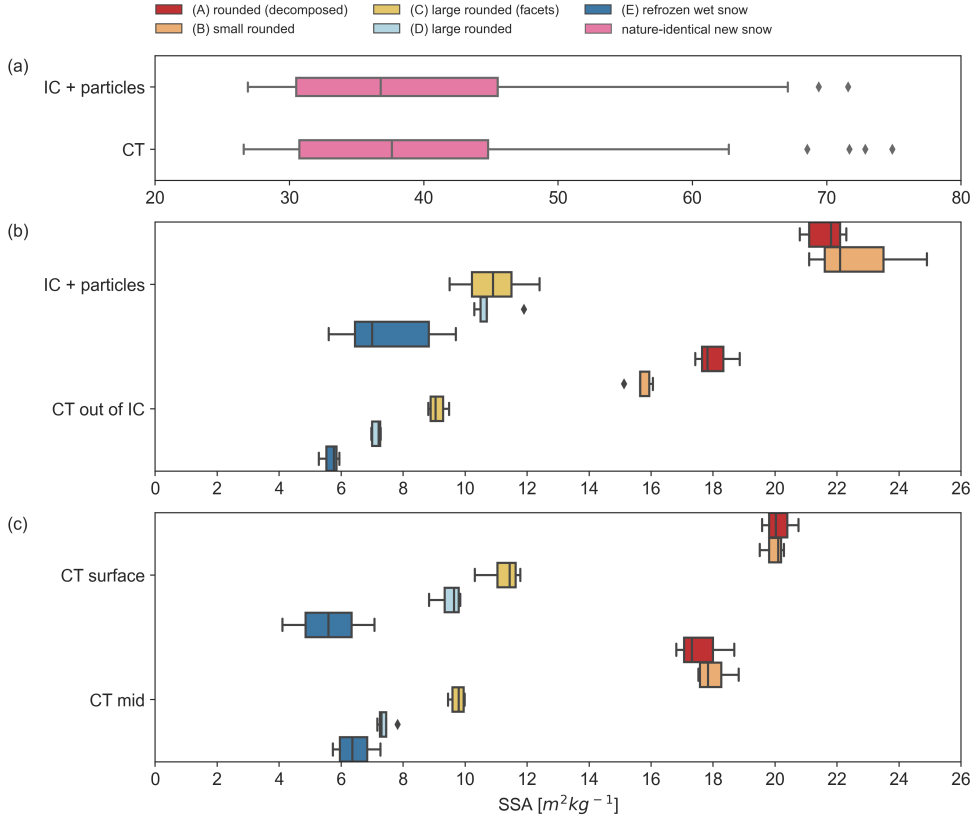


**Figure 1.** All SSA measurements classified in sampling steps. On the left for the artificial snow data set subdivided in IC and CT. SSA in range of 30 to $80\,\mathrm{m^2\,kg^{-1}}$. In the middle the 5 snow types (A,B,C,D,E) subdivided in sampling steps. SSA in range of 5 to $25\,\mathrm{m^2\,kg^{-1}}$. IC + particles is the default sampling process (Gallet et al., 2009; A2 Photonic Sensors, 2014). Results for the micro-CT sampling kit are on the right. SSA in range of 5 to $22\,\mathrm{m^2\,kg^{-1}}$. The results can be found in Tab. A1.

https://doi.org/10.5194/egusphere-2022-501
Preprint. Discussion started: 27 June 2022


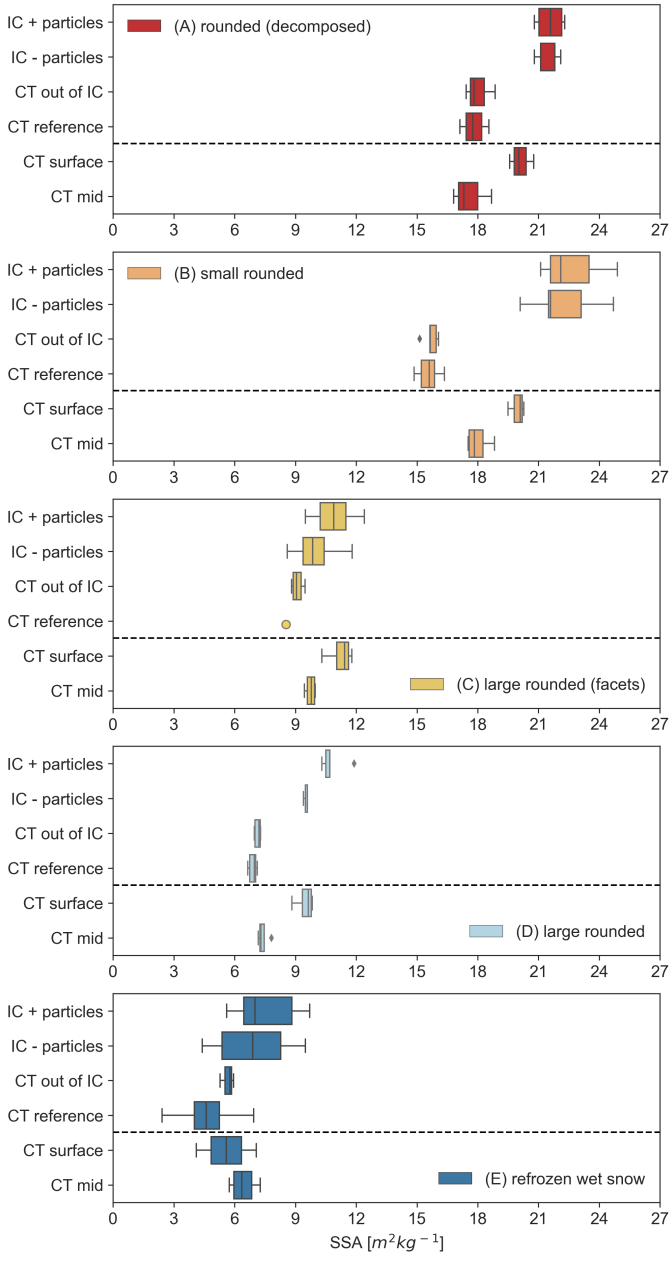


**Figure 2.** All SSA measurements classified in snow types and subdivided sampling steps. SSA in range of 5 to 25 $\mathrm{m^2\,kg^{-1}}$. IC + particles is the default sampling process (Gallet et al., 2009). Results for the micro-CT sampling kit separated by the dotted grey line in each plot. SSA in range of 5 to 22 $\mathrm{m^2\,kg^{-1}}$. The results can be found in Tab. 3.

https://doi.org/10.5194/egusphere-2022-501
Preprint. Discussion started: 27 June 2022


**Table 1.** Means, standard deviations and number of measurements (n) for all measurements organized following the multi-leveled sampling strategy. All calculations and simulations are based on this data set. IC + particles represents the default sampling procedure suggested by Gallet et al. (2009). The line with $\rho^*_{layer}$ is the synthetic density used for the TARTES simulations.

| | **Unit** | **A** | (n) | **B** | (n) | **C** | (n) | **D** | (n) | **E** | (n) |
|---|---|---|---|---|---|---|---|---|---|---|---|
| $\overline{SSA}$ (IC + particles) | $m^2\,kg^{-1}$ | $21.6 \pm 0.6$ | (5) | $22.6 \pm 1.5$ | (5) | $10.9 \pm 1$ | (8) | $10.8 \pm 0.6$ | (5) | $7.5 \pm 1.7$ | (6) |
| $d_{opt}$ (IC + particles) | µm | 303 | | 289 | | 603 | | 605 | | 872 | |
| $\overline{SSA}$ (IC - particles) | $m^2\,kg^{-1}$ | $21.5 \pm 0.5$ | (5) | $22.2 \pm 2.8$ | (5) | $10 \pm 1$ | (8) | $9.5 \pm 0.1$ | (5) | $6.9 \pm 2$ | (6) |
| $d_{opt}$ (IC - particles) | µm | 304 | | 295 | | 661 | | 687 | | 951 | |
| $\overline{SSA}$ (CT out of IC) | $m^2\,kg^{-1}$ | $18 \pm 0.6$ | (5) | $15.7 \pm 0.4$ | (5) | $9.1 \pm 0.3$ | (8) | $7.1 \pm 0.1$ | (5) | $5.7 \pm 0.3$ | (3) |
| $d_{opt}$ (CT out of IC) | µm | 363 | | 417 | | 720 | | 916 | | 1155 | |
| $\overline{SSA}$ (CT reference | $m^2\,kg^{-1}$ | $17.8 \pm 0.6$ | (5) | $15.6 \pm 0.6$ | (5) | 8.5 | (1) | $6.9 \pm 0.2$ | (5) | $4.6 \pm 1.7$ | (5) |
| $d_{opt}$ (CT reference) | µm | 367 | | 420 | | 767 | | 948 | | 1409 | |
| **Micro-CT sampling kit** | | | | | | | | | | | |
| $\overline{SSA}$ (CT surface) | $m^2\,kg^{-1}$ | $20.1 \pm 0.6$ | (3) | $20 \pm 0.4$ | (4) | $11.2 \pm 0.7$ | (4) | $9.5 \pm 0.5$ | (4) | $5.6 \pm 2.1$ | (2) |
| $d_{opt}$ (CT surface) | µm | 325 | | 328 | | 582 | | 689 | | 1170 | |
| $\overline{SSA}$ (CT mid) | $m^2\,kg^{-1}$ | $17.6 \pm 1$ | (3) | $18 \pm 0.5$ | (4) | $9.8 \pm 0.3$ | (4) | $7.4 \pm 0.3$ | (4) | $6.4 \pm 0.7$ | (4) |
| $d_{opt}$ (CT mid) | µm | 372 | | 363 | | 671 | | 884 | | 1017 | |
| **Grain survey)** | | | | | | | | | | | |
| grains (measured) | | 500 | | 1582 | | 997 | | 1962 | | 1130 | |
| $\overline{M}_{part}$ | g | $0.11 \pm 0.02$ | (5) | $0.22 \pm 0.05$ | (5) | $0.72 \pm 0.26$ | (8) | $0.85 \pm 0.17$ | (5) | $2.22 \pm 0.97$ | (6) |
| $SSA_{med}$ (grain survey) | $m^2\,kg^{-1}$ | $14 \pm 5$ | | $49 \pm 32$ | | $72 \pm 57$ | | $85 \pm 58$ | | $61 \pm 36$ | |
| $d_{opt}$ (grain survey) | µm | $461 \pm 172$ | | $133 \pm 92$ | | $91 \pm 64$ | | $77 \pm 49$ | | $107 \pm 65$ | |
| specific mass | $kg\,m^{-2}$ | 0.04 | | 0.08 | | 0.25 | | 0.3 | | 0.8 | |
| **TARTES** | | | | | | | | | | | |
| $SSA_{layer}$ | $m^2\,kg^{-1}$ | 14 | | 49 | | 72 | | 85 | | 61 | |
| $\rho^*_{layer}$ | $kg\,m^{-3}$ | 200 | | 200 | | 200 | | 200 | | 200 | |
| $SSA_{substrate}$ | $m^2\,kg^{-1}$ | 18 | | 16 | | 9 | | 7 | | 6 | |
| $\rho_{substrate}$ | $kg\,m^{-3}$ | 233 | | 420 | | 326 | | 449 | | 312 | |

https://doi.org/10.5194/egusphere-2022-501
Preprint. Discussion started: 27 June 2022


### 3.1 Grain counting

We examined the size and number of the particles formed at the surface of the micro-CT sampling kit (Tab. 3). Table 3 contains the counted number of grains and the weight of particles in the Petri dish. The weight of particles, all measured on the same surface area, varies between $0.11\,\mathrm{g}$ to a maximum of $2.22\,\mathrm{g}$, corresponding to an specific mass of $0.04\,\mathrm{kg\,m^{-2}}$ and $0.8\,\mathrm{kg\,m^{-2}}$, respectively. The calculated particle median SSA ($\mathrm{SSA}_{med}$ (grain survey), Tab. 3) is the lowest for type A ($14 \pm 5\,\mathrm{m^2\,kg^{-1}}$) and the highest for type D ($85 \pm 58\,\mathrm{m^2\,kg^{-1}}$). It is $49 \pm 32\,\mathrm{m^2\,kg^{-1}}$ for type B, $72 \pm 57\,\mathrm{m^2\,kg^{-1}}$ for type C and $61 \pm 36\,\mathrm{m^2\,kg^{-1}}$ for type E. All snow types have a left-skewed particle size distribution. The median optical diameter ($\mathrm{d}_{opt}$ (grain survey)) is between $77 \pm 49\,\mu\mathrm{m}$ to $133 \pm 92\,\mu\mathrm{m}$, except for type A ($461 \pm 172\,\mu\mathrm{m}$). We found an increasing ratio between the optical diameter of the CT reference and the particles as follows: Type A:0.80, B: 3.2, C: 8.4, D: 12.3, E: 13.2. The optical diameter of the particles is smaller than the optical diameter of the undisturbed snow, except for the rounded snow (Type A). The ratio and the size strongly indicate that the sample preparation leads to new small ice particles at the surface. The larger particles of rounded snow (Type A) are just at the limit of statistical significance.

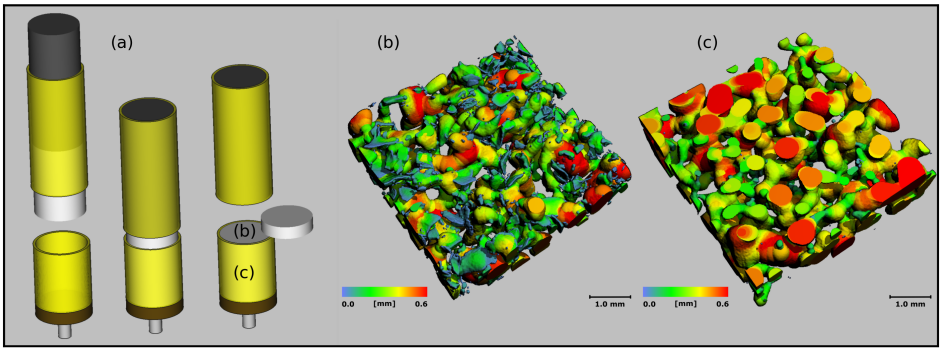


**Figure 3.** Manufactured micro-CT sampling kit (a) and 3D reconstruction for snow type D. Measurements were performed with $\mu$CT80 ($55\,\mathrm{kVp}$, $15\,\mu\mathrm{m}$, $145\,\mu\mathrm{A}$). (b) is the sample surface scan with artificial particles (<$0.5\,\mathrm{mm}$). (c) the snow grains (>$0.5\,\mathrm{mm}$) scanned in the middle of the sample without influence of mechanical treatment.

### 3.2 TARTES

Figure 4 (a) displays the influence of the converted SSA with increasing thickness of the particle layer. Fig. 4 (b) shows the percentage change in SSA with increasing particle thickness. Both layers have different SSA and density values ($SSA_{substrate}$ and $\rho_{substrate}$, Tab. 3). The TARTES simulations (Fig. 4a) show the SSA at $1310\,\mathrm{nm}$ and $950\,\mathrm{nm}$ wavelengths. Figure 4b shows the percentage change in SSA for $1310\,\mathrm{nm}$ and $950\,\mathrm{nm}$ over increasing particle layer thickness. The SSA for $1310\,\mathrm{nm}$ shows a steeper increase with layer thickness compared to $950\,\mathrm{nm}$. The SSA of snow type A shows a slight negative trend with an increase in thickness because the particle layer SSA is smaller than the substrate SSA. The plot on the right shows the percentage change in SSA for $1310\,\mathrm{nm}$ and $950\,\mathrm{nm}$ over increasing particle layer thickness. The starting point at 100% marks

https://doi.org/10.5194/egusphere-2022-501
Preprint. Discussion started: 27 June 2022


the pure substrate SSA for each snow type. The SSA measured at a wavelength of 1310 nm is much more susceptible to the influence of a layer with loose particles. The changes are most prominent for snow types D and E. The slope is about four times higher at 1310 nm than at 950 nm wavelength.

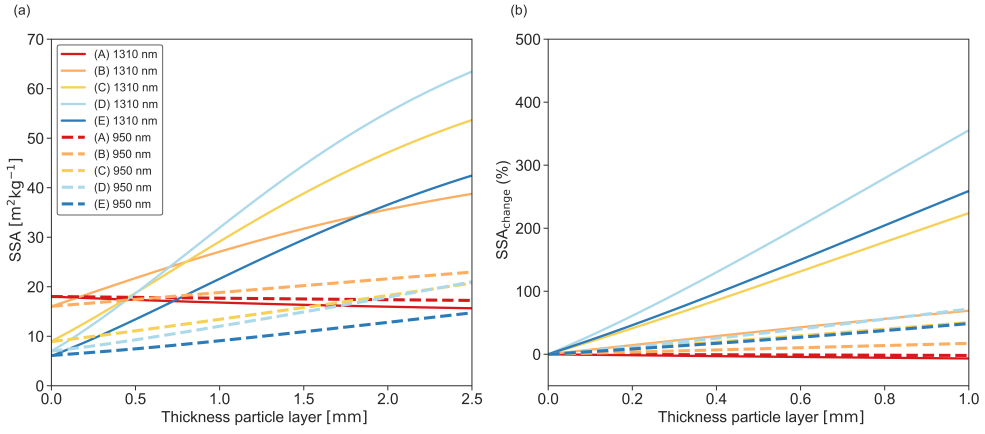


**Figure 4.** Simulated is a 1 m thick snow substrate with a thin (< 2.5 mm) particle layer on top with a density of 200 kg m$^{-3}$. Both layers have different SSA values (Tab.3). The TARTES simulations (a) show the SSA at 1310 nm and 950 nm wavelength. (b) shows the percentage change in SSA for 1310 and 950 nm over increasing particle layer thickness.

## 4 Discussion

We found systematic differences between the IC and the micro-CT SSA measurements for snow with an SSA between 5 m$^2$ kg$^{-1}$ to 25 m$^2$ kg$^{-1}$. The most significant difference appears when the sample is prepared following the default sampling procedure. The relative percentage difference ranges from 52 % for type D (44 % type B, 32 % type E) to 20 % for type A and C. It can be decreased down to 34 % for type D (41 % type B, 21 % type E, 19 % type A) to 9 % for type C by removing loose particles. In contrast, no significant difference can be found in the artificial snow data set with an SSA between 39 m$^2$ kg$^{-1}$ to 80 m$^2$ kg$^{-1}$. We conclude that the observed difference depends on the predisposition of the snow type to produce small surface particles and is not linked to the SSA. We showed that small ice particles form during the flat surface preparation for IC measurements. These particles are preferentially formed from the bonds, as there seems to be a close link to sintering strength. The small particles of the disaggregated snow change the optical properties of the surface and lead consequently to an overestimation of the SSA. It partly corresponds with the observations done by Gallet et al. (2009). They found an overestimation of up to 5 % for hard wind slab layers and suggested brushing the surface to remove particles falsifying the measurement. Gallet et al. (2009) detected an overall accuracy in SSA measurements better than 12 % for the DUFISS device (pre-production model of the IC). Our results indicate that measurements at the wavelength of 1310 nm are prone to systematic biases for most snow types. The micro-CT sampling kit worked well to reconstruct the IC sampling procedure, and the potential layer of artificial particles on the sample surface became visible (Fig. 3). The discrepancies between surface and the sample center in

https://doi.org/10.5194/egusphere-2022-501
Preprint. Discussion started: 27 June 2022


the range of 11 % (type B) to 28 % (type D) support the inference that the number of small particles produced is different for each snow type. The size distributions show most particles to be smaller than 133 µm for types B, C, D and E, which does not correspond with the grain size of the original snow. For each snow type except type A, the survey revealed an optical diameter at least half the size (type B: 133 µm ) compared to the optical diameter estimated from the SSA measured with the IC (type B: 289 µm) and at least three time times smaller then the optical diameter from the CT measurements (type B: 417 µm). For snow of types C, D and E, the $d_{opt}$ is 54 % (type B) up to 88 % (type E) smaller compared to measurements with the IC and 68 % (type B) up to 91 % smaller compared to the CT out of IC measurements. The rounded grain of snow type A appears to be very fragile and does not produce small particles. Consequently, the broken particles are very similar in size to the undisturbed snow. The TARTES simulations show that the albedo at the 950 µm wavelength is more robust and less susceptible towards an artificial particle layer than albedo at 1310 µm. The simulations with 1310 µm can explain the deviation in SSA between the IC and the micro-CT reasonable. For the more fragile snow types C, D and E, a particle layer thickness less than 0.5 mm bridges the deviation. A 1 mm thick particle layer can explain the deviation for the less sensitive snow type B. Type A shows no effect of a particle layer.

## 5 Conclusions

The key to explaining the deviation between IC and micro-CT SSA measurements is the mechanical destruction of parts of the original snow structure into small, artificial particles during the sample preparation process. Those particles lead to an SSA overestimation by the IC. The formation of these particles is related to different variables, such as SSA, temperature, grain shape and sampling treatment. Fresh, poorly bonded snow with a high SSA showed a negligible effect, to a lesser degree also rounded snow. We were able to simulate the effect of the SSA bias with TARTES simulations. The formation of small particles at the surface is a systematic source of bias in spectroscopic measurements. We found that the IC overestimated the SSA and underestimated the optical diameter for most snow types.

*Code and data availability.* The data set and the source code for the TARTES simulation are available on doi:10.16904/envidat.333.

https://doi.org/10.5194/egusphere-2022-501
Preprint. Discussion started: 27 June 2022


## Appendix A

**Table A1.** Table summarizes the statistical analyses. First step was to test for normal distribution. Then testing for significant differences between the sampling steps. Subscript $a$ marks data sets for which at least one is not normal distributed but is assumed for t-testing. IC + particles represents the default sampling procedure suggested by Gallet et al. (2009).

| Snow type | A | B | C | D | E |
|---|---|---|---|---|---|
| Test normal distribution | | | | | |
| IC + particles | Yes | Yes | Yes | Yes | Yes |
| IC - particles | Yes | Yes | Yes | Yes | Yes |
| CT out of IC | Yes | Yes | Yes | Yes | No |
| CT reference | Yes | Yes | No (n<2) | Yes | Yes |
| CT surface | No (n<5) | No (n<5) | Yes | Yes | No (n<3) |
| CT mid | No (n<5) | Yes | Yes | Yes | Yes |
| T-test (one-tailed) | | | | | |
| IC + particles<br>IC - particles | p-value is .40<br>not significant at<br>p<0.05 | p-value is .34<br>not significant at<br>p<0.05 | p-value is .05<br>significant at<br>p<0.05 | p-value is .00<br>significant at<br>p<0.05 | p-value is .29<br>not significant at<br>p<0.05 |
| IC + particles<br>CT out of IC | p-value is .00<br>significant at<br>p<0.05 | p-value is .00<br>significant at<br>p<0.05 | p-value is .00<br>significant at<br>p<0.05 | p-value is .00<br>significant at<br>p<0.05 | p-value is .05<br>not significant at<br>$p<0.05_a$ |
| IC - particles<br>CT out of IC | p-value is .00<br>significant at<br>p<0.05 | p-value is .00<br>significant at<br>p<0.05 | p-value is .01<br>significant at<br>p<0.05 | p-value is .00<br>significant at<br>p<0.05 | p-value is .17<br>not significant at<br>$p<0.05_a$ |
| CT out of IC<br>CT reference | p-value is .30.<br>not significant at<br>p<0.05 | p-value is .38<br>not significant at<br>p<0.05 | none | p-value is .03<br>significant at<br>p<0.05 | p-value is .17<br>not significant at<br>$p<0.05_a$ |
| CT surface<br>CT mid | p-value is .01<br>significant at<br>$p<0.05_a$ | p-value is .00<br>significant at<br>$p<0.05_a$ | p-value is .00<br>significant at<br>p<0.05 | p-value is .00<br>significant at<br>p<0.05 | p-value is .23<br>not significant at<br>$p<0.05_a$ |

| | | | |
|---|---|---|---|
| T-test)<br>(one-tailed) | Nature-identical snow data set | IC<br>CT | p-value is .43<br>not significant at<br>p<0.05 |

https://doi.org/10.5194/egusphere-2022-501
Preprint. Discussion started: 27 June 2022


**Table A2.** Table with equations used in this paper.

| | Parameter | Unit | Equation | Information |
|---|---|---|---|---|
| Weight of particles in petri dish | $M_{part}$ | kg | | measured with scale |
| Optical diameter for particles (assumed to be ellipsoidal) | $d_{opt}$ | m | $\frac{(a+c)}{2}$ | $a$: sphere length $c$: sphere width |
| Surface of particles | $A_{part}$ | $\mathrm{m}^2$ | $4\pi r_{opt}^2$ | |
| Volume of particles | $V_{part}$ | $\mathrm{m}^3$ | $\frac{4}{3}\pi r_{opt}^3$ | |
| Specific mass particle layer | $M_{spec}$ | $\mathrm{kg\,m}^{-2}$ | $\frac{M_{part}}{A_{holder}}$ | $r_{holder} = 0.03\,\mathrm{m}$ |
| SSA of particles | $SSA_{mass}$ | $\mathrm{m}^2\,\mathrm{kg}^{-1}$ | $\frac{A_{part}}{\rho_{ice} V_{part}}$ | |
| Optical diameter | $d_{opt}$ | m | $\frac{6}{\rho_{ice} SSA_{mass}}$ | |

https://doi.org/10.5194/egusphere-2022-501
Preprint. Discussion started: 27 June 2022


*Author contributions.* JM and MS designed the study and conceptualized the data collection. JM carried out the measurements and the simulations and wrote the paper. JM and MS interpreted the results. JM wrote the first draft and MS contributed to the paper.

*Competing interests.* The authors declare that they have no conflict of interest.

*Acknowledgements.* Our sincere thanks goes to Henning Löwe for his ongoing support, enthusiasm and valuable comments.

https://doi.org/10.5194/egusphere-2022-501
Preprint. Discussion started: 27 June 2022


## References

A2 Photonic Sensors: User Manual: IceCube Optical system for the measurement of the specific surface area (SSA) of snow, Tech. rep., www.a2photonicsensors.com, 2014.

Abràmoff, M. D., Magalhães, P. J., and Ram, S. J.: Image processing with imageJ, https://doi.org/10.1201/9781420005615.ax4, 2004.

Domine, F., Taillandier, A. S., and Simpson, W. R.: A parameterization of the specific surface area of seasonal snow for field use and for models of snowpack evolution, Journal of Geophysical Research: Earth Surface, 112, 1–13, https://doi.org/10.1029/2006JF000512, 2007.

Domine, F., Albert, M., Huthwelker, T., Jacobi, H.-W., Kokhanovsky, A. A., Lehning, M., Picard, G., and Simpson, W. R.: Snow physics as relevant to snow photochemistry, Atmos. Chem. Phys. Atmospheric Chemistry and Physics, 8, 171–208, https://doi.org/10.5194/acp-8-171-2008, 2008.

Gallet, J.-C., C., Domine, F., Zender, C., and Picard, G.: Measurement of the specific surface area of snow using infrared reflectance in an integrating sphere at 1310 and 1550 nm, The Cryosphere, 3, 167–182, https://doi.org/10.5194/tc-3-167-2009, 2009.

Gallet, J. C., Domine, F., and Dumont, M.: Measuring the specific surface area of wet snow using 1310 nm reflectance, Cryosphere, 8, 1139–1148, https://doi.org/10.5194/tc-8-1139-2014, 2014.

Hagenmuller, P., Matzl, M., Chambon, G., and Schneebeli, M.: Sensitivity of snow density and specific surface area measured by microtomography to different image processing algorithms, Cryosphere, 10, 1039–1054, https://doi.org/10.5194/tc-10-1039-2016, 2016.

Kerbrat, M., Pinzer, B., Huthwelker, T., Gäggeler, H. W., Ammann, M., and Schneebeli, M.: Measuring the specific surface area of snow with X-ray tomography and gas adsorption: comparison and implications for surface smoothness, Atmospheric Chemistry and Physics Discussions, 7, 10 287–10 322, https://doi.org/10.5194/acpd-7-10287-2007, 2007.

Libois, Q., Picard, G., France, J. L., Arnaud, L., Dumont, M., Carmagnola, C. M., and King, M. D.: Influence of grain shape on light penetration in snow, Cryosphere, 7, 1803–1818, https://doi.org/10.5194/tc-7-1803-2013, 2013.

Morin, S., Domine, F., Dufour, A., Lejeune, Y., Lesaffre, B., Willemet, J. M., Carmagnola, C. M., and Jacobi, H. W.: Measurements and modeling of the vertical profile of specific surface area of an alpine snowpack, Advances in Water Resources, 55, https://doi.org/10.1016/j.advwatres.2012.01.010, 2013.

Schneebeli, M. and Johnson, J. B.: A constant-speed penetrometer for high-resolution snow stratigraphy, Tech. rep., https://doi.org/doi:10.3189/1998AoG26-1-107-111, 1998.